energies

MDPI

Article

Model-Based Algorithm for Flexible Power Point Tracking for Photovoltaic Participation in Primary Frequency Regulation

Loredana Cristaldi [1], Marco Faifer [1], Christian Laurano [1,*], Emil Petkovski [1], Ferdinanda Ponci [2], Igor Sowa [2] and Sergio Toscani [1]

[1] Dipartimento di Elettronica, Informazione e Bioingegneria, Politecnico di Milano, 20133 Milan, Italy; loredana.cristaldi@polimi.it (L.C.); marco.faifer@polimi.it (M.F.); emil.petkovski@polimi.it (E.P.); sergio.toscani@polimi.it (S.T.)

[2] Institute for Automation of Complex Power Systems, E.ON Energy Research Center, RWTH Aachen University, 52074 Aachen, Germany; fponci@eonerc.rwth-aachen.de (F.P.); isowa@eonerc.rwth-aachen.de (I.S.)

* Correspondence: christian.laurano@polimi.it

Abstract: Grid-connected photovoltaic (PV) systems are commonly designed for maximum energy production. However, as their presence grows, revised grid regulations increasingly require these systems to partially adhere to the primary frequency regulation (PFR) by reducing their power production when the grid frequency exceeds the nominal value. Nevertheless, full participation in PFR of PV systems, without battery storage, would require operating with a dedicated active power reserve to be utilized in the event of underfrequency conditions. This paper presents a model-based (MB) flexible power point tracking (FPPT) algorithm for PV systems. Results of a microgrid simulation show that the proposed algorithm enables a PV system with a nominal power of 100 kW to maintain a 20 kW active power reserve under various irradiation and temperature conditions, with a relative error lower than 3%. Furthermore, a simulation of the PV system assisting in primary frequency regulation is presented. Thanks to the proposed strategy, when employing the algorithm, the frequency deviation is reduced both in the event of underfrequency and overfrequency conditions. By enabling operation with a constant active power reserve, as well as a quick adjustment of the produced active power, in the event of frequency imbalance, the proposed MB algorithm is an interesting candidate for achieving complete PFR capabilities of PV systems.

Keywords: photovoltaic systems; microgrids; frequency regulations; maximum power point trackers; flexible power point trackers

Citation: Cristaldi, L.; Faifer, M.; Laurano, C.; Petkovski, E.; Ponci, F.; Sowa, I.; Toscani, S. Model-Based Algorithm for Flexible Power Point Tracking for Photovoltaic Participation in Primary Frequency Regulation. *Energies* **2024**, *17*, 2049. https://doi.org/10.3390/en17092049

Academic Editors: Enrique Romero-Cadaval and Philippe Leclère

Received: 24 January 2024
Revised: 31 March 2024
Accepted: 24 April 2024
Published: 25 April 2024

1. Introduction

In the last decade the growth of renewable energy sources (RES) has been mainly pushed by the rising concern for global warming. Every international crisis, such as the current Russia–Ukraine conflict has resulted in a massive increase in the cost of oil and gas. This event has accelerated the process of substitution of fossil energy sources with the RES. In this direction, the renewable power capacity has grown by 276 GW and 294 GW in 2020 and 2021, respectively [1]. In particular, PV accounts for 134 GW and 151 GW beating the wind capacity addition (112 GW and 93 GW) and hydropower (18 GW and 29 GW). A massive expansion is expected in the PV sector in the upcoming years, reaching a yearly added installed capacity of 350–400 GW in 2026 and 460 GW in 2027 [2]. Therefore, PV technology will play a key role in the energy transition toward sustainable and green energy market.

The big increase in the share of RES in the energy mix of sources installed in the network requires a new and proper control strategy of these resources to guarantee the power network stability. This is particularly true in the case of microgrids where typically RES are the main energy source. As a result, the regulation authorities introduced some requirements for PV plants to partially participate in primary frequency regulation, mainly

by cutting the power production when the grid frequency is higher than nominal [3,4]. This can be easily achieved using traditional hill-climbing methods by imposing an upper limit for the produced power, so that further maximum power point tracking (MPPT) is disabled once this point is reached. On the other hand, different constant power generation strategies are proposed and compared in [5,6] that enable working at reduced power, without providing the knowledge of the maximum power point (MPP) and the available power reserve at any given moment.

In traditional power plants, primary frequency regulation consists of the fast inertial response followed by a chosen droop control. However, this behavior cannot be reproduced by PV power plants operating at the Maximum Power Point (MPP) or with constant power generation strategies. The limitation of such strategies is that while they can be used in transmission systems for the goal of reducing frequency to the nominal value, they cannot be used for the opposite task, as the latter requires availability and knowledge of the active power reserve.

In previous works, the authors have presented a model-based tracking algorithm, allowing a PV system to generate predefined reduced power (RP) [7,8], without any measurement of solar radiation. The proposed flexible power point tracker (FPPT) forces the system to work at a reduced power (as a percentage of the MPP) while maintaining accurate MPP estimation even while working at a reduced power point (RPP). The algorithm was characterized by using a dataset of characteristic curves of a real PV panel acquired over a period of 6 months [7]. The high accuracy of the proposed algorithm was demonstrated for a wide range of irradiation and temperature, for a setting point of the generated power ranging from 20% to 100% of MPP [9].

In this paper, the MB algorithm has been improved to enable RPP operation together with a frequency dependent active power reserve. Afterwards, the feasibility of the MB algorithm in the context of grid frequency regulation is demonstrated in a simulated microgrid scenario. The implemented simulation consists of a grid-forming inverter (GFM), one 75 kW load, two 25 kW loads and a 100 kW PV system connected to the AC grid through a two-stage configuration. Two scenarios are performed.

Firstly, it is shown that the FPPT algorithm can maintain a stable power reserve of 20 kW with a low relative error in different irradiation and temperature working conditions. Secondly, the participation of PV in PFR is demonstrated, simulating underfrequency and over frequency events, by adding or removing an active power load from the microgrid. Results show that the frequency deviation reductions in both the event of overfrequency and underfrequency conditions. It has to be highlighted that, differently from the other proposed FPPTs, the proposed algorithm does not require irradiation measurement or additional reference modules, it can assist both in overfrequency and underfrequency events, it is tested in variable operating conditions, and it does not oscillate between the MPP and the steady-state reduced power point. Thanks to the flexibility of the proposed MB algorithm, by acquiring a first dataset of V-I curves, it can be theoretically adopted for different panel technologies and sizes.

In Section 2, the FPPT algorithm is reported, while in Section 3, the simulated microgrid including the PV system is described, also underlining the implemented modification required for the FPPT integration in the grid frequency regulation control. In Section 4, the results are then reported and discussed.

2. Model-Based Algorithm for Flexible Power Point Tracking

2.1. Literature Review

In recent years, the research on the employment of a flexible power tracking has been boosted by the new energetic scenario. In fact, some countries have recently introduced grid codes for the connection of PV plants to the MV network, trying to regulate and monitor the penetration of those plants in the power grid. On the other hand, the flexibility of a power point tracker would decrease the impact of the unpredictability of the generation.

Different methods have been proposed in order to reserve power for frequency regulation, described in [6,10]. The first considers the use of battery or other energy storage systems or the installation of dump loads to dissipate excessive power [11–13]. Combining PVs with battery energy storage allows us to exploit at maximum the PV system generation but highly increases the plant cost [14]. A more interesting approach entails the operation of the PVs in power curtailment mode, while maintaining an estimate of the MPP, by modifying MPPT algorithms, so that a portion of output power is available for the network and specifically when the frequency must be increased. Despite the loss in production, this kind of operation of PVs may become beneficial and even necessary in some power systems scenarios with a dominant renewable energy fraction. Several recent works present the feasibility of participation of PV plants in grid frequency regulation by means of these types of control strategies [15–17].

In [18], a multi-string system is considered, using one string as the reference to evaluate the maximum available PV power, while the other strings operate at a reduced power. This solution suffers from the well-known problem related to the mismatch of the panels resulting in an estimation error. Other approaches require us to perturbate the working point to evaluate PV parameters necessary for the control such as open-circuit voltage, or the actual maximum power (MP) [19]. This approach results in a continuous oscillation of the system, reducing its efficiency. Other methods perform an estimation of the MP thanks to the measurement of solar radiation and PV cell temperature [20–22], together with curve fitting strategies [23–25]. However, the need for irradiation and temperature sensors increases the system cost and complexity and cannot be performed in dynamic irradiation conditions, such as partially clouded days.

2.2. Proposed Strategy

MB algorithms have been employed to enhance the tracking speed and the dynamic performance of the MPPT. As MB methods are based on the electrical behavior of the panel, in general, they are complex and could require a non-negligible computational burden.

The authors have already proposed a simplified MB algorithm [26], linear in the parameters, that can completely avoid radiation measurement:

$$V_{MP} = A_0 + A_1 T_P + A_2 \ln(I_{MP}) + A_3 \ln^2(I_{MP}). \quad (1)$$

where T_P is the panel temperature, I_{MP} and V_{MP} the MP voltage and current, and A_0–A_3 are the panel parameters derived by the single-diode model of the panel.

If the MP voltages and currents are not known, Equation (1) can be iteratively applied to reach the MPP with a limited number of iterations. It has been demonstrated that the MB MPPT reaches similar results compared to traditional algorithms in steady-state weather conditions, while reaching a better dynamic performance thanks to the limited number of iterations required for the convergence.

To evaluate the value of the A_0–A_3 parameters, a database of the panel has to be acquired, and the estimation procedure can be exploited by employing a weighted least squares approach [26]. In this case, the PV panel is robust and can be employed also during partial shading conditions, and it minimizes the energy loss.

When a point different from the maximum power point has to be tracked, it is straightforward to adapt the MB-MPPT algorithm to reach a desired RPP. Introducing the curtailment factor of the voltage K_V and the current K_I,

$$K_V = \frac{V_{RP}}{V_{MP}};\ K_I = \frac{I_{RP}}{I_{MP}}, \quad (2)$$

Equation (1) can be manipulated as follows:

$$V_{RP} = K_V V_{MP} = K_V \left(A_0 + A_1 T_P + A_2 \ln\left(\frac{I_{RP}}{K_I}\right) + A_3 \ln^2\left(\frac{I_{RP}}{K_I}\right)\right). \quad (3)$$

As far as the RPP current is similar to the MPP current, the MPP can be estimated in a single step, and the voltage is reduced by the factor K_V. As for the MPPT, by implementing Equation (3) iteratively by substituting the actual value of the current I to I_{RP}, the tracking voltage will converge to V_{RP} with any desired power ratio, as presented in [9].

It is worth to underline that this method is robust with respect to the value of K_I and to dynamic conditions in the leftmost part of the characteristic, in which the current value is almost flat and so the two logarithms do not significantly differ when $V < V_{MP}$. Therefore, the power curtailment efficiency mostly depends on the estimation of K_V and on the uncertainty of the employed MPP model (1).

From previous works, it has been demonstrated that the FPPT algorithm provides remarkable performance when it is required to allow a certain percentage of the maximum power point (between 20% and 100%) as a power reserve, allowing the system to achieve an error lower than 2.5% over 6 months of observation [9]. Unfortunately, the power reserve is not constant, but it depends on the theoretical available power, which is variable and unpredictable in time.

Starting from the previous results, this paper improves the proposed MB algorithm to enable operation with a constant active power reserve under different working conditions, as would be preferred in practical applications. This is possible thanks to the inherent property of the MB algorithm to maintain an accurate estimate of the MPP, while operating at reduced power; with this new feature, the power reserve is kept constant enabling the operation in any weather condition. Furthermore, a droop control was implemented, determining the target amount of reserve power, based on the grid frequency.

Differently from the other algorithms presented in the literature, the proposed MB algorithm

- Can assist both overfrequency and underfrequency events;
- Does not require the measurement of irradiation, or additional reference modules to perform FPPT;
- Can operate in variable weather and load condition;
- Is able to directly track a power point without oscillation between the MPPT and FPPT.

3. Numerical Verification

3.1. Microgrid

Microgrids are a fast-growing research topic that have been studied in recent years due to their potential to address several challenges of future grid when comparing to classical power system structures. AC, DC and hybrid microgrids, as well as clusters of those, are able to provide increased reliability and flexibility, strengthening the central grid, while at the same time lowering energy costs for businesses and bringing economic value to local communities [27,28]. In the presented test case, the simulated microgrid consists of two three-phase DC/AC inverters, one grid following (GFL) inverter and one grid forming (GFM) inverter, one 75 kW load, and two 25 kW loads (Figure 1). A 100 kW PV plant is also connected to the AC grid through a two-stage configuration (DC/DC boost plus DC/AC 3-phase inverter).

Grid-forming inverters are essential for AC microgrid applications due to their ability to establish operation in islanded mode, enhance system stability and resiliency especially when a microgrid is dominated by intermittent RES interfaced by power electronics. GFM inverters fulfill their role by directly controlling the voltage at their output terminals, which distinguishes them from grid following inverters that rather control injected currents at their terminals. Additionally, GFM inverters effectively regulate voltage and frequency for other devices in islanded operation, including no-load conditions, while the GFL inverters require reference angle for injection of their currents.

In this exemplary microgrid, the internal control of GFM inverter is designed with voltage and current loops as described in Figure 2.

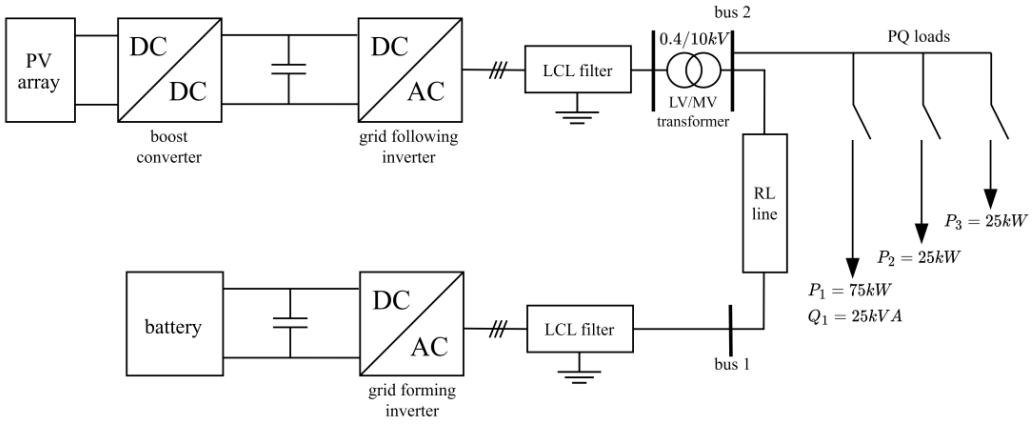

Figure 1. Simulated microgrid.

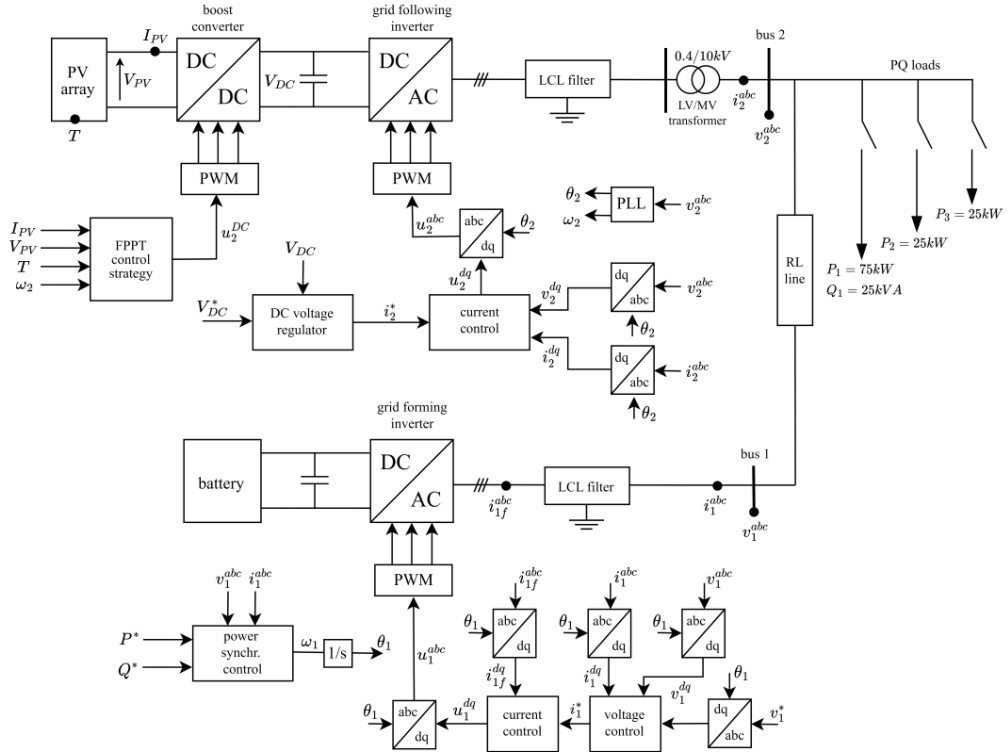

Figure 2. Grid-forming and grid-following inverters control.

It mimics the behavior of synchronous generators in classical power systems according to the droop equation:

$$\omega_1 = \omega_n + D_p(P^* - P) \tag{4}$$

where nominal frequency ω_n equals $2\pi f_n$, D_p is the droop coefficient, P^* is the desired power, while P is the instantaneous measurement of the active power which is calculated from output voltages and currents ($v_1{}^{abc}$, $i_1{}^{abc}$) at bus 1. The synchronization angle θ_1 is obtained by integration of ω_1. Such a structure does not need a dedicated PLL-based synchronization unit during normal operation.

Besides outer power synchronization loop with droop equation, the internal control of GFM inverter consists of current and voltage loops that ultimately produce the required PWM signals according to the measured output voltages and currents.

The control scheme of the grid following a DC/AC inverter that interfaces the PV system is also presented in Figure 2. The AC output current of the GFL inverter is regulated

by the internal current loop, where the reference current i_2* is derived in the DC voltage regulation block,

$$i_2^* = K_p(V_{DC} - V_{DC}^*) + K_i\phi_i \quad (5)$$

$$\dot{\phi}_i = v_{2d}^* - v_{2d}, \quad (6)$$

based on the error of output voltage of the boost converter (VDC), which in turn depends on duty cycle and on reference value V^*_{DC}; K_{cp} and K_{ci} are the current controller PI regulator coefficients. The duty cycle of the IGBT on the boost converter is controlled by the maximum and flexible power tracker of the PV system.

3.2. PV System

The 100 kW PV plant consists of 330 panels divided into 66 strings, each composed of 5 panels. The panels are nominally identical; their characteristics are synthesized in Table 1.

Table 1. PV panel characteristics.

Property	Value
Open-circuit voltage	64.2 V
Short-circuit current	5.96 A
Nominal power (G = 1000 W/m^2; T = 25 °C)	305.226 W
Number of cells	96
Ideality factor	0.945
Temperature coefficient of V_{OC}	−0.2727%/°C
Temperature coefficient of I_{SC}	0.0617%/°C

To train the MB algorithm, 1000 I-V curves of the PV system operating under a random combination of irradiation (G) and temperature (T) conditions have been generated from a real acquired dataset [26]. More specifically, for every I-V curve, one random value of irradiation (in W/m^2) was sampled from a normal distribution with a mean of 700 W/m^2 and standard deviation of 150 W/m^2. Additionally, one value was sampled for temperature (in °C) from a normal distribution with a mean of 25 °C and a standard deviation of 10 °C. Then, the $A_0 \div A_3$ coefficients are estimated, following the procedure described in [28]. Since the complete I-V curves have been synthesized, the values for the voltage and current ratios K_V and K_I could be easily calculated in any power point. In particular, power ratios between 50% and 100% of the MPP have been considered, with a resolution of 1%. For every power ratio (K_P), the mean value of 1000 values of K_V and K_I have been calculated from the dataset. As explained in Section 2, it has been chosen to work on the left side of the characteristic for stability reasons. The values of K_V and K_I as a function of K_P are shown on Figures 3 and 4, respectively.

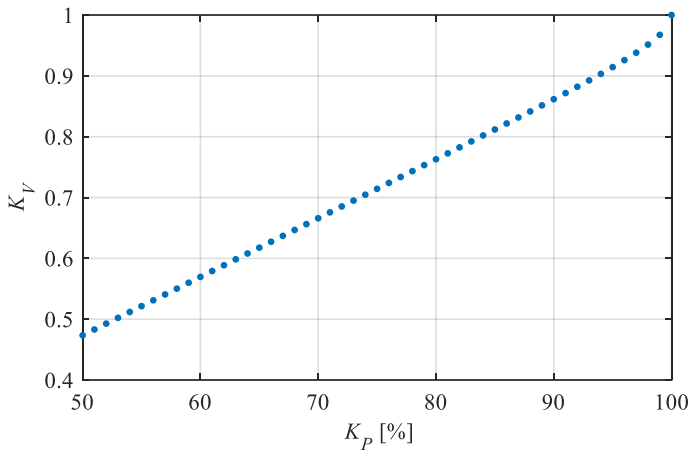

Figure 3. Mean value of voltage ratio coefficient K_V against K_P.

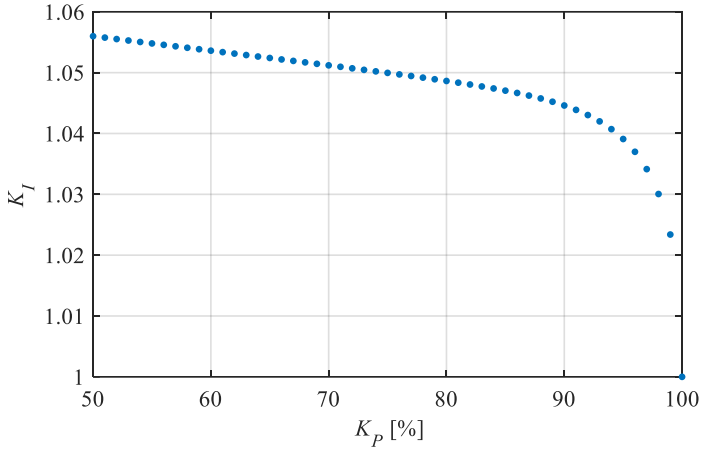

Figure 4. Mean value of current ratio coefficient K_I against K_P.

Once the K_V and K_I have been calculated, the MB algorithm enables working at a reduced power, while maintaining an accurate estimate of the MP. This opens the possibility to establish a constant power reserve. As an example, in this paper, it has been decided to maintain a margin of 20% of the nominal power, corresponding to 20 kW. The best value of the power reserve is case- and market-dependent, as it is linked to the potential revenue that the producer forgoes to be able to provide grid services and to the revenue for the grid services or more in general to the security of operation of the microgrid.

The implemented control strategy based on the FPPT equation onto a DC/DC boost converter (for a two-stage configuration) is shown in Figure 5. With the voltage and current ratios, it is possible to reduce the power output by up to 50% of the MP available. However, the MP value is constantly changing with the ambient conditions (temperature, irradiation), while it is necessary that the desired active power reserve remains constant.

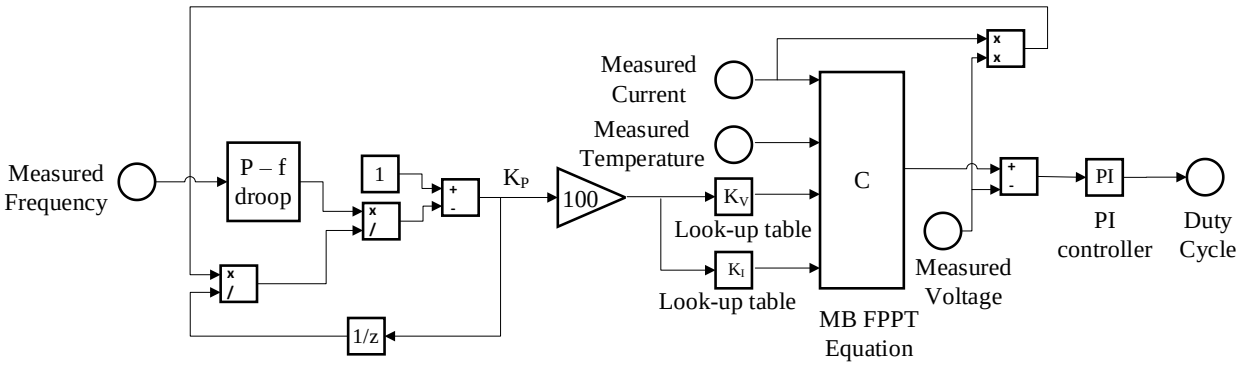

Figure 5. FPPT control strategy.

Considering that the reduced power is equal to the maximum power subtracted by the reserve power P_{res} and that the power ratio K_P is defined as the ratio between the RP and MP (corresponding to P_{MP}), the following equation can be written:

$$K_P = 1 - \frac{P_{res}}{P_{MP}} \tag{7}$$

As shown in [8], in a few iterations, the MB equation accurately converges to the MP under various working conditions. Therefore, considering the implemented control, a change in the ambient conditions will result in a change in the MP and, of course, a change in the instantaneous value of the RP. This in turn will result in an adjustment of the value of K_P. Iteratively, the division of produced RP and K_P will converge to the new MP, and

through Equation (7), the correct value of K_P will be determined, so that the necessary power reserve is maintained.

Hence, through the maximum power estimate, the correct K_P is determined, following the changes in the environmental conditions. K_P is then passed to the look-up tables resulting in the updating of the K_V and K_I values to maintain the constant power reserve. Linear interpolation has been used to interpolate between the data.

The MB equation requires the measurement of current and temperature as well as the K_V and K_I values of the panel and regulates the reference voltage. Once the reference voltage is known, the duty cycle is set by the PI controller to adjust the actual voltage value. The schematic is shown in Figure 5.

4. Results and Discussion

To validate the proposed algorithm, different simulations have been performed. Firstly, the capability of the MB FPPT algorithm to maintain a stable power reserve of 20 kW in different working conditions was validated. Afterwards, the participation of PV in PFR was analyzed, simulating underfrequency and overfrequency scenarios, by connecting or disconnecting a 25 kW load, respectively.

4.1. Maintaining a Constant Power Reserve

In order to demonstrate that the FPPT algorithm can maintain a desired active power reserve under various environmental conditions, it was necessary to replicate the working condition of a PV system during a clear day. To that end, the irradiation on a panel and its temperature were measured on the roof of a building at Politecnico di Milano. Their profiles are represented by the blue curves on Figure 6a,b. Afterwards, applying linear interpolation, approximated daily irradiation and temperature profiles were obtained, to be used in simulation. They are represented by the red curves of Figure 6a,b. Using the approximated daily profiles, a second simulation was executed two times. In the first instance, the PV system performed using the MB MPPT algorithm, while in the second instance, the FPPT with a desired reserve of 20 kW has been selected. The difference between the produced power and MP under the different environmental conditions is shown in Figure 6c. It shows that throughout a typical clear day, the algorithm can maintain an active power reserve of 20 kW with an error smaller than 600 W, or a relative error smaller than 3%.

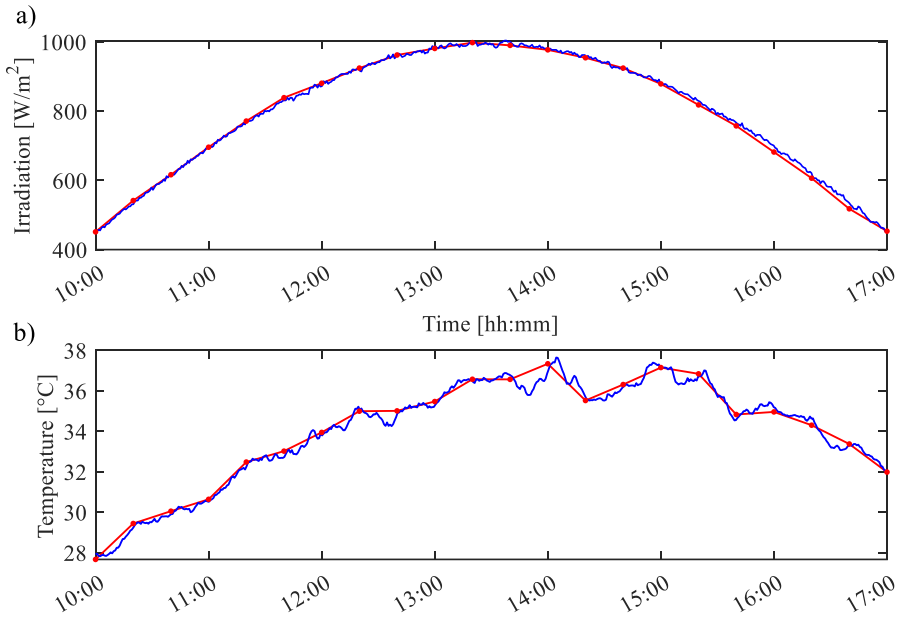

Figure 6. *Cont.*

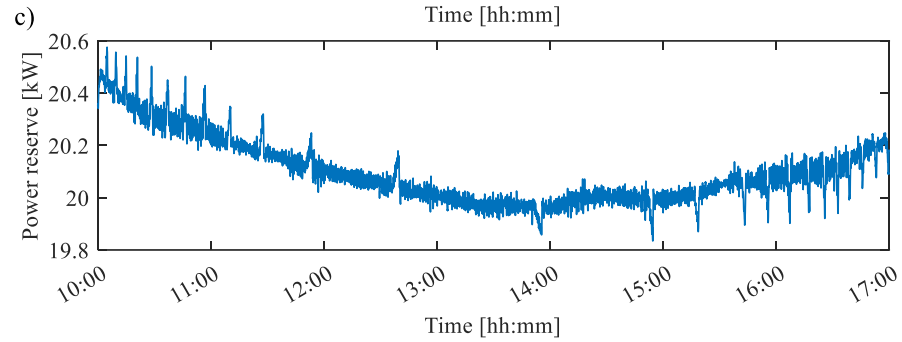

Figure 6. (**a**) Irradiation profile, (**b**) temperature profile (measured values in blue line and interpolated values in red line), (**c**) maintained active power reserve.

4.2. Primary Frequency Regulation

Once the ability of the algorithm to maintain an active power reserve has been established, the second objective of the paper was to realize a PFR scenario, for a set of ambient conditions. PV plant operation under irradiation of 900 W/m^2 and a temperature of 30 °C was selected, typical for the central part of the day. The PV system provides P = 67.6 kW, working with a 20.25 kW margin. Since the desired reserve at nominal frequency is 20 kW, this means that the system is operating with a relative error of 1.25%. The connected loads require 100 kW of active power. Therefore, the rest of the power demand is met by the grid forming inverter. Both the scenarios of underfrequency and overfrequency have been simulated. Moreover, both the conditions with the PV participating or not in the PFR have been simulated and compared.

The droop curve of the PV system is presented in Figure 7. When the system frequency reduces, the injected power increases, by utilizing the power kept in reserve. The system reaches MP output for the frequency of 49.6 Hz. The opposite happens in the case of a frequency increase, which results in less power injected by the PV. Power kept in the reserve reaches 40 kW, for a frequency of 50.4 Hz. A similar droop is implemented for the grid-forming inverter, designed to provide 32 kW at the nominal frequency of 50 Hz.

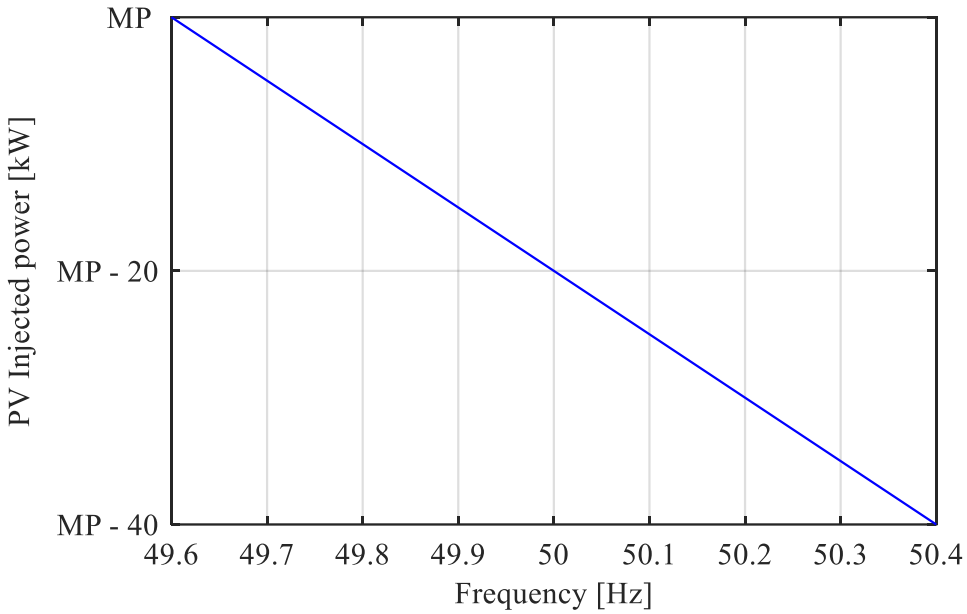

Figure 7. Implemented active power–frequency droop control.

First of all, when the simulation starts, the PV is working with the traditional MB algorithm at its maximum power, which corresponds to 87.85 kW. After 0.2 s of simulation time, the operator requires the PV to operate with a power reserve of 20 kW, by implement-

ing the correct curtailment factors and the PV system reduces its output to the previously mentioned value of 67.65 kW. The additional power is provided by the battery connected to the grid forming inverter, and in fact, the output frequency remains stable to the nominal value. At t = 0.5 s of simulation time, the droop control is enabled, resulting in a very slight frequency drop, as the grid forming inverter is providing slightly more power than 32 kW.

First, the simulation of a load connection is carried out. In this case, after t = 1 s, an additional load of 25 kW is connected, creating a power imbalance, consequently resulting in an underfrequency condition. The transient dynamic has been evaluated, resulting in reaching the new steady state condition in less than 0.2 s.

Figure 8 shows the dynamic response of the microgrid frequency based on whether the PV system participates or not in PFR, while Figure 9 shows the power output of the PV system in both cases.

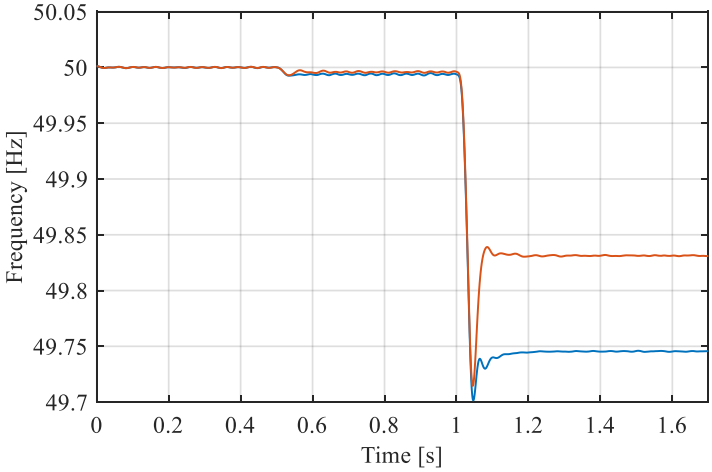

Figure 8. Frequency behavior during a load connection with (red line) or without (blue lines) PV system participating to PFR.

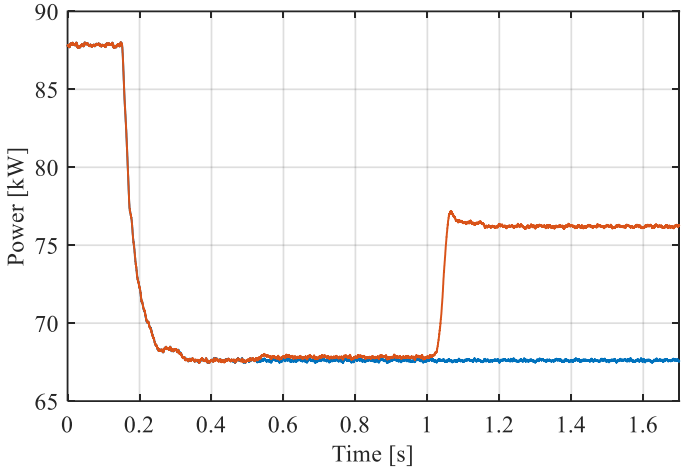

Figure 9. PV power injection during a load connection with (red line) or without (blue lines) PV system participating to PFR.

From the figures, we can see the consistency of the participation of the PV in the frequency regulation. In fact, when the PFR of the PV system is enabled, it increases its power output from 67.6 kW to 76.21 kW, and as a result, the frequency of the system drops to 49.831 Hz as opposed to 49.746, when the control is not enabled and only the GFM inverter is forced to completely supply the additional load, decreasing the frequency reduction from 5% (when the PV does not participate in frequency regulation) to 3.4% (when the PV is able to sustain the grid frequency).

Moreover, the overfrequency scenario has also been realized similarly to the previous scenario, by disconnecting a 25 kW load after 1 s of simulation time. Results in terms of frequency and power are provided in Figures 10 and 11.

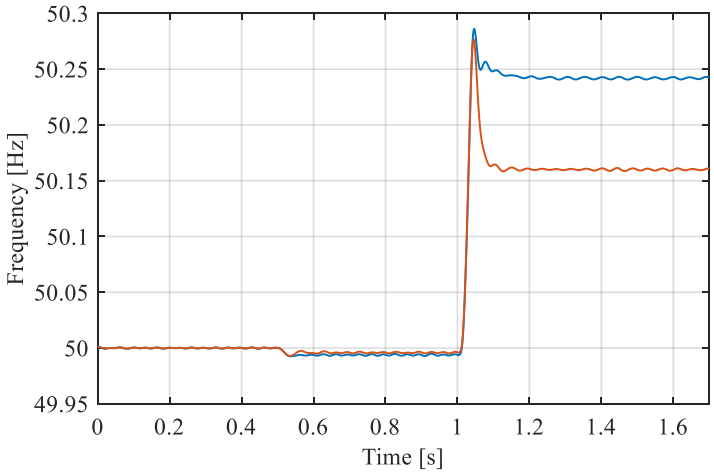

Figure 10. Frequency behavior during a load disconnection with (red line) or without (blue lines) the PV system participating in the PFR.

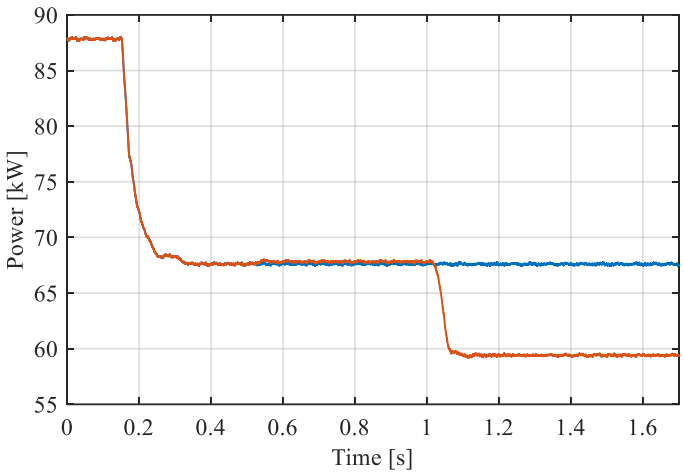

Figure 11. PV power injection during a load disconnection with (red line) or without (blue lines) the PV system participating in the PFR.

Again, the effectiveness of the solution is evident. In fact, when the PV system participates in the regulation, the output power is automatically reduced from 67.6 kW to 59.4 kW. Thanks to the power injection reduction, the frequency rise is dampened to a value of 50.16 Hz, as opposed to 50.242 Hz, when the control is not enabled (in relative terms from +4.8% to +3.2%). Both the performances during load connection and disconnection are summarized in Table 2.

Table 2. Comparison of frequency deviations.

Scenario	PV Participation	Frequency Deviation
Load disconnection	No	+4.8%
	Yes	+3.2%
Load connection	No	−5%
	Yes	−3.4%

In summary, during both critical scenarios, the participation of the PV system in the PFR leads to a smaller deviation of the frequency from the nominal value. Furthermore, inverter-based photovoltaic or battery systems can adjust their output power more rapidly than synchronous generators, due to the lack of system inertia and the high switching frequency of the power electronics [29]. Correspondingly, it can be observed that in both presented scenarios, the simulated PV system increases or reduces its produced active power with a transient lower than 0.1 s. This time response is fully compliant with the needs of the TSO for the purpose of primary frequency regulation.

The proposed model-based algorithm has demonstrated to be accurate and reliable in maintaining constant active power reserves in the simulated conditions and quick in adjusting active power output in the case of frequency imbalances. This makes it a highly promising solution for enabling PV systems to achieve full PFR capability and a key step in the complete integration of PVs in grid operability.

5. Conclusions

Full participation in PFR of PV systems will allow the increase in their implementation in the new grid scenario, allowing us to reduce the energy demand from non-renewable energy sources and the impact of the system on global warmth. On the other hand, to reduce the economic impact of PV systems, one can decide to avoid the use of battery storage, but it would require operating with a dedicated active power reserve to be dispatched in the event of underfrequency conditions. This paper presents a model-based FPPT algorithm for PV systems, designed to control their operation between 50% and 100% of MP, along with its model estimation procedure. Differently from the other proposed FPPT algorithms, the proposed algorithm does not require irradiation measurement or additional reference modules, it can assist both in overfrequency and underfrequency events, it has been tested in variable operating conditions, and it does not oscillate between the MPP and the steady-state reduced power point. Moreover, the flexibility of the MB algorithm allow its implementation for any PV technology.

Simulations show that in a microgrid simulation, the MB algorithm enables a 100 kW PV system to maintain a 20 kW active power reserve under various irradiation and temperature conditions. Furthermore, the results demonstrate the PV system participation in the PFR, using the proposed MB control. In the event of a frequency drop, the increased production of the PV system limits the frequency drop in the microgrid. This value cannot be achieved with the current constant power control strategies. Moreover, in the event of a sudden load reduction, the PV system reduces its power output, limiting the frequency rise. Thanks to the accuracy of the model-based algorithm in maintaining a constant active power reserve under various environmental conditions, as well as the rapid active power change in the event of frequency imbalance, it is a very promising candidate for enabling PV systems to fully perform primary frequency regulation.

Author Contributions: Conceptualization, E.P., M.F., C.L., S.T., I.S. and F.P.; methodology, E.P. and F.P.; software, E.P. and I.S.; validation, E.P. and I.S.; formal analysis, C.L., M.F. and L.C.; investigation, E.P. and I.S.; resources, M.F. and F.P.; data curation, E.P. and C.L.; writing—original draft preparation, E.P., M.F., C.L. and I.S.; writing—review and editing, M.F., E.P., L.C., C.L. and F.P.; visualization, I.S. and E.P.; supervision, M.F., C.L., S.T., L.C. and F.P. All authors have read and agreed to the published version of the manuscript.

Funding: This research received no external funding.

Data Availability Statement: The original contributions presented in the study are included in the article, further inquiries can be directed to the corresponding author.

Conflicts of Interest: The authors declare no conflicts of interest.

References

1. IEA. Renewables 2022: Analysis and Forecast to 2027. 2023. Available online: https://iea.blob.core.windows.net/assets/ada7af90-e280-46c4-a577-df2e4fb44254/Renewables2022.pdf (accessed on 23 April 2024).

2. Solar Power Europe. Global Market Outlook for Solar Power 2022–2026. 2022. Available online: https://api.solarpowereurope.org/uploads/Solar_Power_Europe_Global_Market_Outlook_report_2022_2022_V2_2_87bd2c1e44.pdf (accessed on 23 April 2024).
3. Seidel, J.; Rauscher, F.; Engel, B. Enhanced contribution of photovoltaic power systems to frequency control in future Power Systems. *IET Renew. Power Gener.* **2021**, *15*, 2753–2765. [CrossRef]
4. Energinet.dk. *Technical Regulation 3.2.2 for PV Power Plants with a Power Output above 11 kW*; Technical Repert No. 14/17997-39; Energinet.dk: Fredericia, Denmark, 2016.
5. Sangwongwanich, A.; Yang, Y.; Blaabjerg, F.; Wang, H. Benchmarking of Constant Power Generation Strategies for Single-Phase Grid-Connected Photovoltaic Systems. *IEEE Trans. Ind. Appl.* **2018**, *54*, 447–457. [CrossRef]
6. Tafti, H.D.; Konstantinou, G.; Townsend, C.D.; Farivar, G.G.; Sangwongwanich, A.; Yang, Y.; Pou, J.; Blaabjerg, F. Extended Functionalities of Photovoltaic Systems with Flexible Power Point Tracking: Recent Advances. *IEEE Trans. Power Electron.* **2020**, *35*, 9342–9356. [CrossRef]
7. Cristaldi, L.; Faifer, M.; Laurano, C.; Petkovski, E.; Toscani, S.; Ottoboni, R. An Innovative Model-Based Algorithm for Power Control Strategy of Photovoltaic Panels. In Proceedings of the IEEE International Instrumentation and Measurement Technology Conference (I2MTC), Ottawa, ON, Canada, 16–19 May 2022; pp. 1–6. [CrossRef]
8. Cristaldi, L.; Faifer, M.; Laurano, C.; Ottoboni, R.; Petkovski, E.; Toscani, S. Reduced Power Model-Based Tracker for Photovoltaic Panels. In Proceedings of the IEEE International Conference on Compatibility, Power Electronics and Power Engineering (CPE-POWERENG), Birmingham, UK, 29 June–1 July 2022; pp. 1–6. [CrossRef]
9. Cristaldi, L.; Faifer, M.; Laurano, C.; Ottoboni, R.; Petkovski, E.; Toscani, S. Power Generation Control Algorithm for the Participation of Photovoltaic Panels in Network Stability. *IEEE Trans. Instrum. Meas.* **2023**, *72*, 9000809. [CrossRef]
10. Narang, A.; Farivar, G.G.; Tafti, H.D.; Pou, J. Power Reserve Control Methods for Grid-Connected Photovoltaic Power Plants: A Review. In Proceedings of the 2022 IEEE 7th Southern Power Electronics Conference (SPEC), Nadi, Fiji, 5–8 December 2022; pp. 1–5. [CrossRef]
11. Hill, C.; Such, M.C.; Chen, D.; Gonzalez, J.S.; Grady, W.M. Battery Energy Storage for Enabling Integration of Distributed Solar Power Generation. *IEEE Trans. Smart Grid* **2012**, *3*, 850–857. [CrossRef]
12. Ma, W.; Wang, W.; Wu, X.; Hu, R.; Tang, F.; Zhang, W.; Han, X.; Ding, L. Optimal Allocation of Hybrid Energy Storage Systems for Smoothing Photovoltaic Power Fluctuations Considering the Active Power Curtailment of Photovoltaic. *IEEE Access* **2019**, *7*, 74787–74799. [CrossRef]
13. Shivashankar, S.A.; Mekhilef, S.; Mokhlis, H.; Karimi, M. Mitigating Methods of Power Fluctuation of Photovoltaic (PV) Sources—A Review. *Renew. Sustain. Energy Rev.* **2016**, *59*, 1170–1184. [CrossRef]
14. Rajan, R.; Fernandez, F.B.; Yang, Y. Primary Frequency Control Techniques for Large-Scale PV-Integrated Power Systems: A Review. *Renew. Sustain. Energy Rev.* **2021**, *144*, 110998. [CrossRef]
15. Poliak, O.; Shmilovitz, D. Power Reserve from Photovoltaics for Improving Frequency Response in the Isolated System. *Energies* **2023**, *16*, 3595. [CrossRef]
16. Tafti, H.D.; Konstantinou, G.; Fletcher, J.; Callegaro, L.; Farivar, G.G.; Pou, J. Control of Distributed Photovoltaic Inverters for Frequency Support and System Recovery. *IEEE Trans. Power Electron.* **2022**, *37*, 4742–4750. [CrossRef]
17. Sharma, S.; Jately, V.; Kuchhal, P.; Kala, P.; Azzopardi, B. A Comprehensive Review of Flexible Power-Point-Tracking Algorithms for Grid-Connected Photovoltaic Systems. *Energies* **2023**, *16*, 5679. [CrossRef]
18. Sangwongwanich, A.; Yang, Y.; Blaabjerg, F.; Sera, D. Delta Power Control Strategy for Multistring Grid-Connected PV Inverters. *IEEE Trans. Ind. Appl.* **2017**, *53*, 3862–3870. [CrossRef]
19. Sangwongwanich, A.; Yang, Y.; Blaabjerg, F. Sensorless Reserved Power Control Strategy for Two-Stage Grid-Connected Photovoltaic Systems. In Proceedings of the 2016 IEEE 7th International Symposium on Power Electronics for Distributed Generation Systems (PEDG), Vancouver, BC, Canada, 27–30 June 2016; pp. 1–8. [CrossRef]
20. Gomez, J.M.; Shanmugam, P.K. Flexible Power Point Tracking Using a Neural Network for Power Reserve Control in a Grid-Connected PV System. *Energies* **2022**, *15*, 8234. [CrossRef]
21. Li, Q.; Baran, M. A Novel Frequency Support Control Method for PV Plants Using Tracking LQR. *IEEE Trans. Sustain. Energy* **2020**, *11*, 2263–2273. [CrossRef]
22. Verma, P.; Kaur, T.; Kaur, R. Power Control Strategy of an Integrated PV System for Active Power Reserve under Dynamic Operating Conditions. *Sustain. Energy Technol. Assess.* **2021**, *45*, 101066. [CrossRef]
23. Wang, Z.; Yi, H.; Zhuo, F.; Lv, N.; Ma, Z.; Wang, F.; Zhou, W.; Liang, J.-F.; Fan, H. Active Power Control of Voltage-Controlled Photovoltaic Inverter in Supporting Islanded Microgrid without Other Energy Sources. *IEEE J. Emerg. Sel. Top. Power Electron.* **2021**, *10*, 424–435. [CrossRef]
24. Batzelis, E.; Kampitsis, G.; Papathanassiou, S.A. Power Reserves Control for PV Systems with Real-Time MPP Estimation via Curve Fitting. *IEEE Trans. Sustain. Energy* **2017**, *8*, 1269–1280. [CrossRef]
25. Batzelis, E.; Papathanassiou, S.A.; Pal, B.C. PV System Control to Provide Active Power Reserves under Partial Shading Conditions. *IEEE Trans. Power Electron.* **2018**, *33*, 9163–9175. [CrossRef]
26. Cristaldi, L.; Faifer, M.; Laurano, C.; Ottoboni, R.; Toscani, S.; Zanoni, M. Model-based maximum power point tracking for photovoltaic panels: Parameters identification and training database collection. *IET Renew. Power Gener.* **2020**, *14*, 2876–2884. [CrossRef]

27. Chen, B.; Wang, J.; Lu, X.; Chen, C.; Zhao, S. Networked Microgrids for Grid Resilience, Robustness, and Efficiency: A Review. *IEEE Trans. Smart Grid* **2021**, *12*, 18–32. [CrossRef]
28. Al-Ismail, F.S. DC Microgrid Planning, Operation, and Control: A Comprehensive Review. *IEEE Access* **2021**, *9*, 36154–36172. [CrossRef]
29. *NERC Fast Frequency Response Concepts and Bulk Power System Reliability Needs*; NERC Inverter-Based Resource Performance Task Force (IRPTF); NERC: Alanta, GA, USA, 2020; pp. 1–23. Available online: https://www.nerc.com/comm/PC/InverterBased%20Resource%20Performance%20Task%20Force%20IRPT/Fast_Frequency_Response_Concepts_and_BPS_Reliability_Needs_White_Paper.pdf (accessed on 23 April 2024).